

# ULTRAVIOLET-VISIBLE ACOUSTO-OPTIC TUNABLE SPECTROSCOPIC IMAGER FOR MEDICAL DIAGNOSIS

G. C. Tang,<sup>†‡</sup> J. T. Chen,<sup>‡</sup> Alvin Katz,<sup>‡</sup> Edward J. Celmer,<sup>\*</sup> Ronald W. Krumm,<sup>†</sup> and R. R. Alfano<sup>‡</sup>

<sup>†</sup>Mediscience Technology Corp., P.O. Box 598, Woodcrest, Cherry Hill, New Jersey 08003 and 49 Willow Place, Albertson, New York 11507; <sup>‡</sup>The City College of New York of CUNY, Institute for Ultrafast Spectroscopy and Lasers Mediphotonics Laboratory, New York, New York 10031; <sup>\*</sup>St. Vincent's Medical Center of Richmond, Department of Pathology, Staten Island, New York 10310

(Paper JBO-152 received Apr. 14, 1997; revised manuscript received Aug. 12, 1997; accepted for publication Oct. 7, 1997.)

## ABSTRACT

An ultraviolet to visible acousto-optic tunable filter was used to measure native fluorescence images from *in vitro* breast tissues at different wavelengths. Pseudocolor maps based on fluorescence images at two wavelengths were used to separate normal and abnormal regions in human breast tissues *in vitro*, providing diagnostic information. © 1998 Society of Photo-Optical Instrumentation Engineers. [S1083-3668(98)00701-1]

**Keywords** acousto-optic tunable filter; breast tissues; fluorescence images; diagnostic information.

## 1 INTRODUCTION

Over the past decade, progress has been achieved toward developing less invasive diagnostic approaches based on fluorescence spectroscopy using native fluorophores of tissues in the ultraviolet (UV) and visible spectral regions.<sup>1-10</sup> These changes in fluorescence spectra arise from both the presence of different molecules and the structural changes that occur in tissue. Several optical algorithms have been employed to detect differences between malignant and normal tissues in the visible and UV spectra. These methods include taking the ratio of emitted intensities at two (or more) emission or excitation wavelengths; taking the spectral intensity difference at two (or more) emission or excitation wavelengths, and observing if the difference exists above or below a predetermined value; or comparing the spectral profile obtained from a measured sample with an averaged spectral profile computed from a large number of tissue samples.

The use of 300-nm excitation has made it possible to discern differences between malignant and normal or benign breast,<sup>4</sup> gynecological,<sup>5</sup> and colon tissue samples.<sup>6</sup> The emission intensity ratio at 340 to 440 nm has been used as a diagnostic indicator.<sup>4,5</sup> Based on measurements from large numbers of human tissue samples,<sup>5-9</sup> the ratios from most of the cancer *in vitro* samples lie well above a critical num-

ber, while benign and normal tissue ratios lie well below this value. The difference in fluorescence intensity ratios can be used to distinguish between cancerous and normal tissues. The 340-nm emission arises from tryptophan, while the 440-nm emission is a composite arising from collagen, elastin, and reduced nicotinamide adenine dinucleotide phosphate (NADH). Current measurements indicate that the combined use of emission, excitation, and scattering spectra, with multiple wavelengths, increases diagnostic accuracy.<sup>6</sup>

To implement these spectroscopic approaches in medical applications, measurements need to be performed rapidly. Acousto-optical tunable filter (AOTF) devices offer a programmable, rapidly changeable spectroscopic tool that has been under development for more than two decades.<sup>11</sup> It offers the potential of rapidly acquiring spectral images at multiple wavelengths.<sup>12</sup> An AOTF has a much higher switching speed than liquid-crystal tunable filters (LCTF), diffraction gratings, and movable interference filters,<sup>13</sup> and AOTFs have the capability of working in the UV spectral region.

This paper describes a novel fluorescence spectral imaging technique that is based on an acoustic optical tunable filter to map the fluorescence intensity ratio at a pair of wavelengths over an area of tissue. A pseudocolor ratio map of the tissue area is used to highlight changes in the tissue's architecture and morphology.

Address all correspondence to R. R. Alfano. Tel: (212) 650-6960; Fax: (212) 650-5530; E-mail: alfano@scisun.sci.cny.cuny.edu

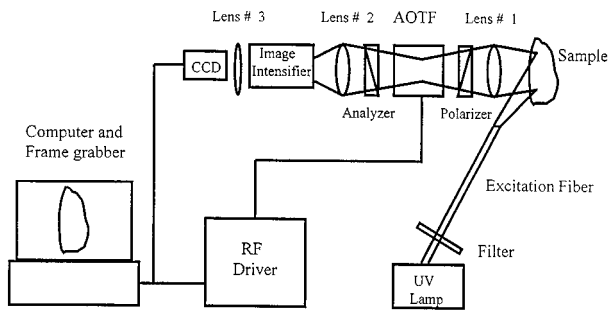


**Fig. 1** Schematic diagram of AOTF fluorescence spectral imaging system.

## 2 METHODS AND SAMPLES

A schematic diagram of the AOTF spectral imaging system is shown in Figure 1. A noncollinear geometry AOTF device was obtained from Brimrose Corp. (Baltimore, Maryland). The optical aperture is  $7 \times 7$  (mm<sup>2</sup>). The spectral range covers 300 to 500 nm. The drive frequency can be varied from 98 MHz to 53 MHz. The acceptance angle (total) is 5.3 to 7.3 deg. Spectral resolution is 3.5 nm at 300 nm, and 18.4 nm at 475 nm. Test data indicated a diffraction efficiency of 6% and an out-of-band rejection of 3:1. The excitation source is a high-intensity xenon lamp with a 300-nm narrow band filter with a 10-nm bandwidth and 15% transmission coupled into a liquid light guide for delivery to the sample. The liquid light guide has a 5-mm diameter with about 60% transmission at 300 nm. The fluorescence from the sample was collected and imaged on the AOTF by a UV imaging lens. Placing the AOTF at the image plane minimized the divergence of the collected light. Two WG-320 Schott glass filters were used to eliminate scattered excitation light. A second lens transferred the image into an image intensifier. After the signal was amplified by the image intensifier, the fluorescence image was reimaged onto a CCD camera. A Matrox frame grabber installed in a personal computer was used to digitize and further process the image. The controlling software generated and displayed the pseudocolor fluorescence ratio maps.

Pseudocolors were used to represent spectral intensity ratios of the fluorescence map indicating various tissue states for different regions. Different pseudocolor mappings were employed to maximize the visibility of abnormal tissue states. An example of the relationship between the spectral ratio and pseudocolors is given in Table 1. For this case,

**Table 1** Relationship between the ratios and pseudocolors.

| Ratio | <4.5  | 5         | 6    | 7        | 8     | 9      | 10     | 11        | 12  | 13       | 14       | 15   | 16-18     | >18   |
|-------|-------|-----------|------|----------|-------|--------|--------|-----------|-----|----------|----------|------|-----------|-------|
| Color | black | deep blue | blue | sky blue | green | yellow | orange | light red | red | dark red | deep red | gray | deep gray | white |

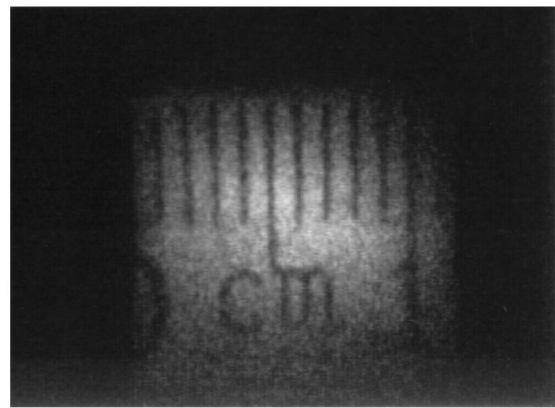


**Fig. 2** Image of scale showing the imaged size of  $1 \times 1$  cm<sup>2</sup>.

the red indicated abnormal ratio readings, while the green and blue indicated ratios that would represent benign or normal regions of tissues.

A background image with no acoustic wave in the AOTF crystal was measured to give a reference level. The background frame was stored in computer memory and directly subtracted from the acquired frame prior to ratioing. The image size and resolution of the map system was measured using a scale and bar chart as shown in Figures 2 and 3, respectively. The image size was  $1 \times 1$  cm<sup>2</sup>, and the spatial resolution at 440 nm was determined to be 2 line pairs/mm.

Breast tissue samples were obtained from the St. Vincent Medical Center of Staten Island, with histological results. Specimens were not chemically treated prior to measurements.

## 3 RESULTS AND DISCUSSION

Several dissection specimens of *in vitro* tissues with a thickness of about 5 mm were measured using the AOTF spectral image mapping system with 300-nm excitation. The fluorescence images from a normal breast tissue are shown in Figure 4 (color plate). The tissue size was about  $8 \times 11$  mm<sup>2</sup>. The image size was about a third of the CCD detector area. The fluorescence intensity ratio,  $I_{340}/I_{440}$ , was independently measured using a fluorescence spectrometer and found to be 2.7. Figure 4(a) shows the image of the 340-nm emission, while Figure 4(b) shows the image of the 440-nm emission. The pseudocolor ratio map for the  $I_{340}/I_{440}$  ratio with a reference color scale is shown in Figure 4(c). For the data in Figure 4(c), the background was subtracted prior to ratioing. One

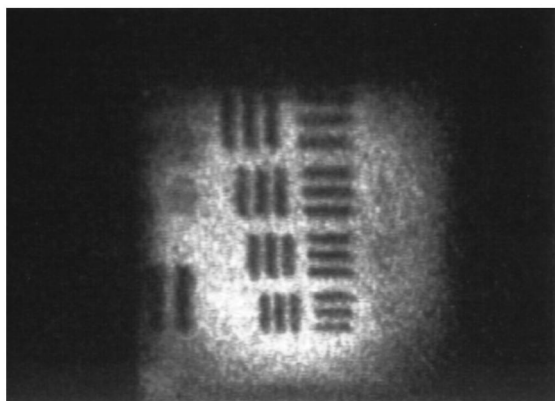


**Fig. 3** Image of bar chart showing the resolution of 2 line pairs per millimeter (0.25 mm).

can see that the pseudocolors in Figure 4(c) are largely blue and deep blue over most areas of the map. Using the reference pseudocolor scale on the left of Figure 4(c), the ratio values for the map are estimated to be below 6, which indicates the sample was a normal tissue. Areas where the signal was weak are shown in black in Figure 4(c). The small yellow and red pixels in the ratio map are due to image intensifier noise.

Fluorescence images were measured on a sample of cancerous breast tissue about  $8 \times 6$  mm. The fluorescence intensity ratio at  $I_{340}/I_{440}$  with 300-nm excitation was measured with a spectrometer and found to be 10.8. The fluorescence images from this sample are displayed in Figure 5 (color plate) for the 340-nm emission [Figure 5(a)] and for the 440-nm emission [Figure 5(b)]. The ratio image map of the  $I_{340}/I_{440}$  over the sample is shown in Figure 5(c) with a reference color scale. The pseudocolor image is red for most of the tissue. Referring to the pseudocolor scale shown on the left side of Figure 5(c), the ratios for the red area in the map are about 12.

In order to test the ability to detect and image small tumors, a small cancerous tissue about 1.5 mm in diameter was placed on top of a large normal breast tissue sample. Figure 6 (color plate) shows the spectral image map of the  $I_{340}/I_{440}$  ratio in a pseudocolor scale. One can clearly see from the map that a small red area exists in the central part of the map. This area represents a high-ratio region, showing the location of the cancer.

Two problems were observed with the current AOTF unit. The first problem was the low transmission efficiency, which was only 6%, four times smaller than the expected value. This may be improved by manufacturing in the future. The second problem was the poor out-of-band rejection by the AOTF, which allowed a large background leakage to interfere with the desired signals. The acceptance angle for the AOTF used in this work was specified to be 5.3 to  $\sim 7.3$  deg. When broadband light was incident on the crystal with angles of incidence up to 7.3 deg, significant background leakage was

transmitted through the system. This background level reduced the extinction ratio, resulting in a smaller dynamic range. Further reducing the collection angle would greatly curtail the weak emission from tissues at 440 nm. One way to reduce the background leakage is to use an AOTF with a larger diffraction angle. In this case, the image, at a selected wavelength, is spatially separated from the incident broadband background. A unit with a diffraction efficiency of 30% and an out-of-band rejection of  $>10^3$  is needed to make useful devices.

A high spatial resolution AOTF with  $0.35 \mu\text{m}$  has been achieved in a microscopy image application.<sup>14</sup> The spatial resolution in our imaging system is about  $250 \mu\text{m}$ , which is reasonable for tissue analysis. The output of the Continuous Wave (CW) light source used in the experiments was only about 1 mW at 300 nm. It could be replaced by a pulsed light source with a larger output in the UV region, which would be useful for biomedical studies.

A major advantage of AOTFs is their ability to rapidly change wavelength (the switching time can be as fast as  $5 \mu\text{s}$ ) since they have a higher frame rate than other spectral devices such as a slowly mechanical filter wheel. At this time, data were acquired at 1 to 2 Hz. During mapping in real time, our software has a function that can capture one frame of background image and temporarily store it in its memory. The software then automatically subtracts the background from each subsequent image and gives a background-corrected ratio map. Although the unit can run at 1 to 2 Hz for a fixed tissue target, the background correction procedure must be repeated for a new tissue region. Performing this procedure takes a few seconds. It could be improved using software for automatic correction.

A liquid-crystal tunable filter<sup>13</sup> is a candidate for a real-time diagnosis instrument in the visible region. Its switch time is about 50 ms, which is much slower than the AOTF. Moreover, the AOTFs can be used in the UV region, while the LCTFs cannot. The Fourier transform spectroscopy approach may be a technology competing with AOTFs for Raman spectroscopic images, but it is difficult to use in real-time fluorescent imaging.

#### 4 SUMMARY

A breadboard AOTF 2-D spectral image map system was used to demonstrate the potential to map fluorescence emission from tissues. The system produced pseudocolor maps that differentiated the value of the fluorescence intensity ratios at two wavelengths over an area of  $1 \text{ cm}^2$ . The separation of cancers from normal zones of *in vitro* tissue was demonstrated. The spatial resolution of the 2-D AOTF-based spectral image map system is on the order of 0.25 mm. At this time, the poor out-of-band rejection and the low transmission efficiency limit the application of the AOTF for *in vivo* tissue work in the UV region.

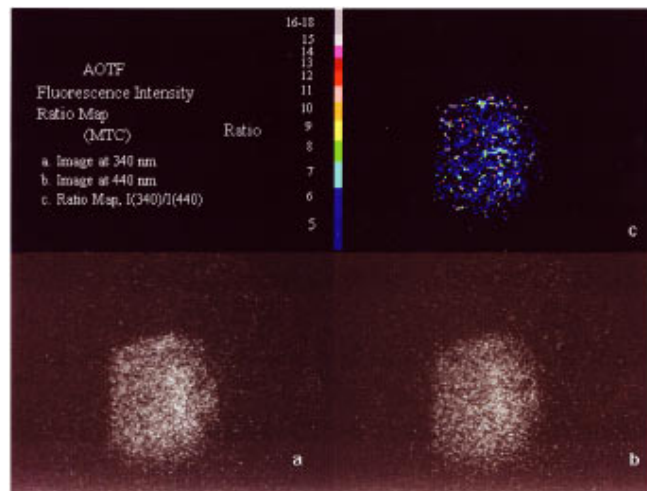


**Fig. 4** Spectral images of normal breast tissue excited at 300 nm, having a ratio of 2.5. (a) Fluorescence image for wavelength at 340 nm, (b) Fluorescence image for wavelength at 440 nm, (c) Ratio map with a discrete pallet.

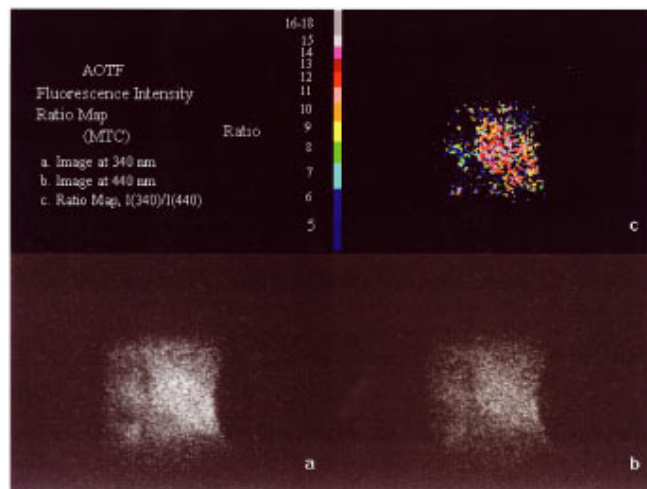


**Fig. 5** Spectral images of cancerous breast tissue excited at 300 nm, having a ratio of 10.5. (a) Fluorescence image for wavelength at 340 nm, (b) Fluorescence image for wavelength at 440 nm, (c) Ratio map with a discrete pallet.

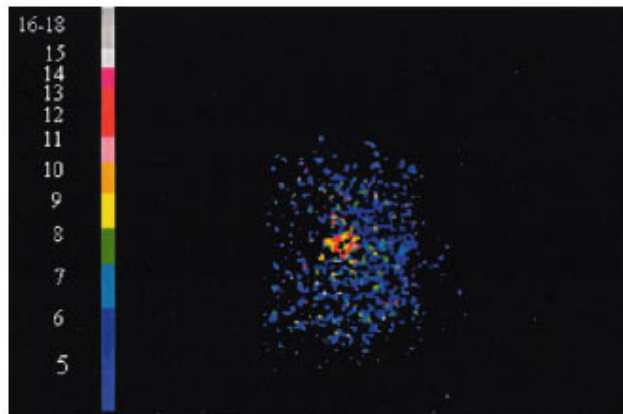


**Fig. 6** Spectral images of a small cancerous breast tissue of 1.5 mm diameter on a larger normal tissue excited at 300 nm.

## Acknowledgment

This research was supported by the Small Business Innovation Research Program of the National Institute of Health, IR43CA62768-01A1, grant to Medicine Technology Corp.

## REFERENCES

1. R. R. Alfano, D. B. Tata, J. J. Cordero, P. Tomashefsky, F. W. Longo, and M. A. Alfano, "Laser-induced fluorescence spectroscopy from native cancerous and normal tissues," *IEEE J. Quant. Electron.*, **QE-20**, 1507-1511 (1984).
2. R. R. Alfano, G. C. Tang, A. Pradhan, W. Lam, and D. S. J. Choy, "Fluorescence spectra from cancerous and normal breast and lung tissues," *IEEE J. Quantum Electron.* **QE-23**, 1806-1811 (1987).
3. G. C. Tang, A. Pradhan, and R. R. Alfano, "Spectroscopic differences between human cancer and normal lung and breast tissues," *Lasers Surg. Med.* **9**, 290-295 (1989).
4. R. R. Alfano, B. B. Das, J. Clearly, R. Prudente, and E. J. Celmer, "Light sheds light on cancer, distinguishing malignant tumor from benign tissue and tumors," *Bull. N.Y. Acad. Med.* **67(2)**, 143 (1991).
5. W. S. Glassman, C. H. Liu, G. C. Tang, S. Lubicz, and R. R. Alfano, "Ultraviolet excited fluorescence spectra from non-malignant and malignant tissues of gynecological tract," *Lasers Life Sci.* **5(1-2)**, 49-58 (1992).
6. Y. L. Yang, G. C. Tang, M. Bessler, and R. R. Alfano, "Fluorescence spectroscopy as a photonic pathology method for detecting colon cancer," *Lasers Life Sci.* **6(4)**, 259-276 (1995).
7. L. J. Deckelbaum, J. K. Jam, H. S. Cabin, K. S. Clubb, and M. B. Lomg, "Discrimination of normal and atherosclerotic aorta by laser-induced fluorescence," *Lasers Surg. Med.* **7**, 330-335 (1989).
8. E. S. Anderson, J. Johansson, K. Svanberg, and S. Svanberg, "Fluorescence imaging and point measurements of tissue: application to the demarcation of malignant tumors and atherosclerotic lesions from normal tissue," *Photochem. Photobiol.* **53**, 807-814 (1991).
9. N. Ramanujam, M. E. Mitchell, A. Mahadevan, S. Thomsen, E. Silva, and R. R. Richards-Kortum, "Fluorescence spectroscopy: a diagnostic tool for cervical intraepithelial neoplasia (CIN)," *Gynecol. Oncol.* **52**, 31-38 (1994).
10. R. M. Cothren, R. R. Richards-Kortum, M. V. Sivak, M. Fitzmaurice, R. P. Rava, G. A. Boyce, G. B. Hayes, M. Doxtader, R. Blackman, T. B. Ivanc, and M. S. Feld, "Gastrointestinal tissue diagnosis by laser-induced fluorescence spectroscopy at endoscopy," *Gastrointest. Endoscopy* **36**, 105-116 (1990).
11. I. C. Chang, "Tunable acousto-optic filter utilizing acoustic beam walkoff in crystal quartz," *Appl. Phys. Lett.* **25**, 323-324 (1974).
12. P. J. Treado, I. W. Levin, and E. N. Lewis, "Indium antimonide (InSb) focal plane array (FPA) detection for near-infrared imaging techniques," *Appl. Spectroscop.* **48**, 607-615 (1994).
13. C. C. Hoyt and D. M. Benson, "Merging spectroscopy and digital imaging enhances cell research," *Photonics Spectra* **26**, 92-96 (1992).
14. E. S. Wachman, W. H. Niu, and D. L. Farkas, "Imaging acoustic-optic tunable filter with micron spatial resolution," *Appl. Opt.* **35**, 5220-5226 (1996).